Strength Verification of a Rotary Curved Plate in a Flow Field

Lei Zhang, Min Gao, Bukui Zhou, Yunfei Liu

Abstract—**We propose a method based on an empirical formula for solving the problem of verifying the strength of a columnar curved plate in a flow field. The deformation equation of the columnar curved plate was established first. Considering the difficulty of the analytical solution, it is assumed that the unilateral curved plate only experiences torsional deformation that is linearly distributed along the exhibition direction, which could reduce motion to a single degree of freedom. Aerodynamic load models with different airspeeds and attack angles were established based on lift line theory and strip assumptions. The failure points and dangerous stress on the columnar curved plates, which are unilaterally fixed, partially connected branches, were obtained using the theory of material mechanics. The results were verified using finite element simulation software. Considering that the dynamic load on the curved plate structure in a flow field is much larger than that of a static load, an empirical relationship between the static and dynamic loads is obtained based on a large number of previous simulation and test results. Taking a certain structure as an example, the dynamic load in the flow field is simulated and analyzed using the empirical formula, which provides a theoretical basis for strength design and analysis of this type of structure.**

Index Terms—**Rotary curved plate; lift line theory; strength checking; finite element; dynamic load**

I. Introduction

COLUMNAR curved panels are widely used in aviation, aerospace, shipbuilding, and civil engineering to build aircraft wing skin structures [1], piezoelectric wind generators [2], wrap-around fins in missiles, blast furnace gas dehydration devices [3], and turbine blades in a turbocharger [4]. These panels have smooth appearance, strong bending and torsional resistance, and are light weight. All the structures mentioned above exist in a flow field environment and with a high-speed rotating working mode, which leads to occasional structural damage resulting from large deformation. Methods for verifying the strength of columnar curved plates under an applied load in a flow field has remained the focus of many researchers [5] . In early studies on the strength of curved panels, many researchers assumed that the curved panel was an ideal homogeneous structure, and the ultimate load of the curved panel was equal to the elastic critical buckling load. Redshaw [6] and Timoshenko [7] obtained different expressions describing the elastic critical buckling stress using the energy method and an approximate expression for the displacement field, respectively. In recent years, the development of finite element software has provided an effective numerical method for analyzing the strength of curved plate structures. Given the lack of a formula in the European Standard for predicting the ultimate load of columnar curved panels, Le Tran [8] used the finite element method to calculate the stability of metallic columnar curved plates and proposed a semi-empirical formula for predicting the ultimate strength of columnar curved plates subjected to axial compressive loads, thus combining the numerical solution with the verification process for plate and shell stability in Euro Code 3. Considering the influence of different structural parameters and boundary conditions on stability, Martins [9], Shariati [10], Han [11], and Sun LY [12] studied the elastic buckling behavior of columnar curved plates using finite element method and through experiments; the various results were consistent with each other. Li [13], Chen [14], and Huan [15] analyzed the stability of composite-stiffened curved panels using experimental and finite element methods. Fan [16-18] studied the defect susceptibility of a composite curved plate and analyzed the influence of different defects on the ultimate load.

Although the results from the finite element method are typically accurate, the finite element method is not applicable in engineering design due to the huge number of required calculations and the long calculation period [19-21].

Based on previous studies, Li [22] proposed a relatively concise engineering method for calibrating the strength of a columnar curved plate, which is consistent with experimental results. However, this method only considers the structural stress of curved plates with different parameters under a certain load and the dynamic strength under different dynamic conditions. Considering a curved plate as an elastic structure in a flow field will redistribute the aerodynamic load; the stress at the failure point will change accordingly, which means that the original verification method will be biased towards failure. Based on classical aeroelastic analysis, this study develops a method for verifying the strength of columnar curved plates with different structural parameters in a flow field in order to provide a theoretical basis for the design of such structures.

Manuscript received October 10, 2018; revised November 19, 2020.

Lei Zhang is an engineer of Defense Engineering, AMS, PLA, BeiJing, 100036, China (e-mail: oeczl99@163.com).

Min Gao is a professor of Army Engineering University, Shijiazhuang, Hebei, 050003, China (e-mail: gaomin1103@yeah.net).

Bukui Zhou is a senior engineer of Defense Engineering, AMS, PLA, BeiJing, 100036, China(corresponding author, e-mail: zbk751225@sina.com)

Yunfei Liu is a senior engineer of Defense Engineering, AMS, PLA, BeiJing, 100036, China (e-mail:liuyff@126.com)

II. Open cylindrical shell deformation model

The open cylindrical shell model is shown in Figure 1. ϕ_0 is an angle that defines curvature, c is the length of a chord, x is the bus on the middle surface, and $s=\varphi\cdot R$ is the circumference. $R=r+b/2$ is the radius of curvature along the direction of the circumference, r is the radius of the missile, and b is the thickness of the wing. E is the elastic modulus and μ is Poisson's ratio. The dimensionless coordinates are $\alpha=x/R$ and $\beta=\varphi$. Stress concentration along the bus and the circumference are ignored in this model, while q_n defines stress concentration along the direction normal to the middle surface.

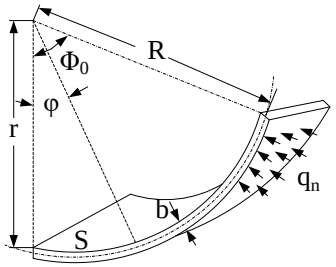

Fig.1 Cylindrical shell model

An auxiliary function $\Phi(\alpha,\beta)$ is introduced, which is used to calculate the displacement components u, v, and w (defined along x, s, and normal to the middle surface, respectively):

$$\begin{cases} u=\dfrac{\partial^3\Phi}{\partial\alpha\partial\beta^2}-\mu\dfrac{\partial^3\Phi}{\partial\alpha^3} \\ w=\nabla^2\nabla^2\Phi \\ v=-(2+\mu)\dfrac{\partial^3\Phi}{\partial\alpha^2\partial\beta}-\dfrac{\partial^3\Phi}{\partial\beta^3} \end{cases} \tag{1}$$

According to the cylindrical shell simplification theory, the deformation problem can be solved by solving the following eight-order partial differential equations under given boundary conditions [8]:

$$\nabla^2\nabla^2\nabla^2\nabla^2\Phi+\frac{\partial^4\Phi}{\partial\alpha^4}=\frac{R^2}{Eb}q_n \tag{2}$$

The boundary condition of the curved plate is unilaterally clamped, and the remaining three sides are free. The auxiliary function is defined in the following three sets of partial differential equations:

$$\begin{cases} \dfrac{\partial^3\Phi}{\partial\alpha\partial\beta^2}-\mu\dfrac{\partial^3\Phi}{\partial\alpha^3}=0 \\ (2+\mu)\dfrac{\partial^3\Phi}{\partial\alpha^2\partial\beta}+\dfrac{\partial^3\Phi}{\partial\beta^3}=0 \\ \dfrac{\partial^4\Phi}{\partial\alpha^4}+2\dfrac{\partial^4\Phi}{\partial\alpha^2\partial\beta^2}+\dfrac{\partial^4\Phi}{\partial\beta^4}=0 \\ \dfrac{\partial^5\Phi}{\partial\alpha^4\partial\beta}+2\dfrac{\partial^5\Phi}{\partial\alpha^2\partial\beta^3}+\dfrac{\partial^5\Phi}{\partial\beta^5}=0 \end{cases} \tag{3}$$

$$\begin{cases} \dfrac{\partial^4\Phi}{\partial\alpha^4}=\dfrac{\partial^4\Phi}{\partial\alpha^3\partial\beta}=0 \\ \dfrac{\partial^6\Phi}{\partial\beta^6}+\dfrac{2\partial^6\Phi}{\partial\alpha^2\partial\beta^4}+\dfrac{\mu\partial^6\Phi}{\partial\alpha^2\partial\beta^4}+\dfrac{\mu\partial^6\Phi}{\partial\alpha^6}=0 \\ \dfrac{\partial^7\Phi}{\partial\beta^7}+\dfrac{(4-\mu)\partial^7\Phi}{\partial\alpha^2\partial\beta^5}+\dfrac{(2-\mu)\partial^7\Phi}{\partial\alpha^6\partial\beta}=0 \end{cases} \tag{4}$$

$$\begin{cases} \dfrac{\partial^4\Phi}{\partial\alpha^2\partial\beta^2}=\dfrac{\partial^6\Phi}{\partial\alpha^6}+\dfrac{(2+\mu)\partial^6\Phi}{\partial\alpha^4\partial\beta^2}+\dfrac{(1+2\mu)\partial^6\Phi}{\partial\alpha^2\partial\beta^4}+\mu\dfrac{\partial^6\Phi}{\partial\beta^6}=0 \\ \dfrac{12(1+\mu)R^2\partial^4\Phi}{b^2\partial\alpha^3\partial\beta}+\dfrac{\partial^6\Phi}{\partial\alpha^5\partial\beta}+\dfrac{\partial^6\Phi}{\partial\alpha^3\partial\beta^3}+\dfrac{\partial^6\Phi}{\partial\alpha\partial\beta^5}=0 \\ \dfrac{\partial^7\Phi}{\partial\beta^7}+\dfrac{(5-2\mu)\partial^7\Phi}{\partial\alpha^3\partial\beta^4}+\dfrac{(4-\mu)\partial^7\Phi}{\partial\alpha^5\partial\beta^2}+\dfrac{(2-\mu)\partial^7\Phi}{\partial\alpha^6\partial\beta}=0 \end{cases} \tag{5}$$

$\Phi(\alpha,\beta)$ can be determined from the set of four equations in equation (3), then we could get displacement u, v, and w. The three strain components on the middle surface can be defined in terms of the moment of a cylindrical shell [8]:

$$\begin{cases} \varepsilon_\alpha=\dfrac{\partial u}{\partial x} \\ \varepsilon_\beta=\dfrac{1}{R}\dfrac{\partial v}{\partial\varphi}+\dfrac{w}{R} \\ \gamma_{\alpha\beta}=\dfrac{1}{R}\dfrac{\partial u}{\partial\varphi}+\dfrac{\partial v}{\partial x} \end{cases} \tag{6}$$

The curvature change and twist rate are

$$\begin{cases} \kappa_1=-\dfrac{\partial^2 w}{\partial x^2} \\ \kappa_2=-\dfrac{1}{R^2}\dfrac{\partial^2 w}{\partial\varphi^2}-\dfrac{w}{R^2} \\ \chi=\dfrac{1}{2R}\left(\dfrac{\partial v}{\partial x}-\dfrac{1}{R}\dfrac{\partial u}{\partial\varphi}-2\dfrac{\partial^2 w}{\partial x\partial\varphi}\right) \end{cases} \tag{7}$$

However, it is difficult to determine the form of the auxiliary function that meets all the boundary conditions in the above model. Therefore, the above equation can only be solved using numerical methods. Therefore, it is necessary to develop a relatively simple alternative model that facilitates engineering strength verification.

III. Unilaterally fixed model

Most curved plate structures are unilaterally fixed and locally connected. Without loss of generality, a structural model can be constructed, as shown in Fig.1. The angle in the spanwise direction is ϕ_0; c_R and c_T are the root string and sharp string, respectively; the section width of the fixed branches is mc_R, which are located at distances p and q away from the front and rear edges of the root, respectively.

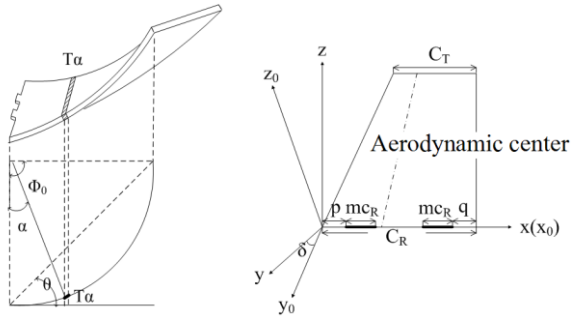

Fig. 1 Unilaterally fixed curved plate model

An analytical solution to the deformation equation describing the plate-shell structure under the action of a specific distributed load is difficult to obtain. Lift line theory is used to simplify the calculation of the aerodynamic load on the aircraft. It is considered that the flow field load of the curved plate is the normal force acting on the lift line at 1/4 the length of the chord.

The curved plate is considered to be composed of a series of strip elements. Regardless of the ternary effect of the fluid along the span direction, the load produced by the flow field load on each strip is assumed to be related only to the local flow velocity and direction[23].

The load produced by the flow field generates a torsion angle β_q at the sharp string. The torsion distribution on the curved plate can be approximated as linear. Therefore, the rotation angle of the strip T_α corresponding to the curvature α should be

$$\beta(\alpha)=\frac{\alpha}{\phi_0}\beta_q=\frac{s}{\phi_0 r}\beta_q \tag{8}$$

Let δ be the angle between the flow direction and the root string. According to the system geometry, the angle between the strip and the incoming flow should be

$$\delta(\alpha)=\sin\delta(\alpha)=\sqrt{1-a^2} \tag{10}$$

This angle appears in the following equation:

$$a=\cos\beta(\alpha)\cos\delta-\sin\beta(\alpha)\cos(\alpha-\frac{\phi_0}{2})\sin\delta \tag{11}$$

According to lift line theory, the load distribution produced by the flow field can be expressed as follows [20]:

$$dL(\alpha)=qca_1\delta(\alpha)rd\alpha \tag{12}$$

The Lagrange method is used to solve the problem according to classical aeroelastic analysis theory, yielding the torsion angle β_q, when the sharp string has an incremental twist angle, there should be an incremental twist angle $d\beta$ on strip T_α:

$$d\beta=\frac{\alpha}{\phi_0}d\beta_q \tag{13}$$

Due to the incremental torsion angle on strip T_α, the incremental work done by the flow field is $dL(\frac{c}{4})d\beta$.

The total incremental work is found by integrating the over the entire curve:

$$\delta W=\int_0^{\phi_0}dL(\frac{c}{4})d\beta=\frac{qc^2a_w rd\beta_q}{4\phi_0}\int_0^{\phi_0}\alpha\delta(\alpha)d\alpha \tag{14}$$

The strain energy corresponding to torsional deformation is

$$U=\frac{1}{2}\int_0^{\phi_0 r}GJ(\frac{d\beta}{ds})^2ds=\frac{GJ}{2\phi_0 r}\beta_q^2 \tag{15}$$

β_q can then be taken as the generalized coordinate and substituted into the Lagrange equation:

$$Q_\theta=\frac{\partial(\delta W)}{\partial(d\beta_q)}=\frac{qc^2a_w r}{4\phi_0}\int_0^{\phi_0}\alpha\delta(\alpha)d\alpha=\frac{\partial(U)}{\partial(\beta_q)}=\frac{GJ}{\phi_0 r}\beta_q \tag{16}$$

β_q can be solved using the above equation and substituted into Eq. (12), yielding the load distribution on the lift line.

IV. STATIC STRENGTH VERIFICATION

During static load strength verification, the load on the curved plate produced by the flow field can be regarded as a combination of a bending moment and torque. Therefore, the bending stress and torsional stress must be calculated separately.

A. Bending stress calculation

Figure 2 shows the coordinate system used to calculate bending stress.

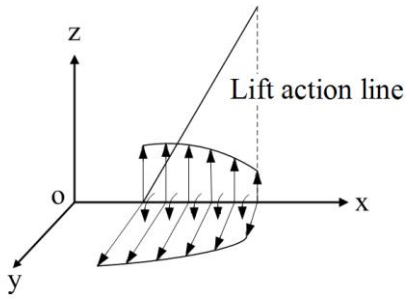

Fig. 2 Flow field load decomposition Lift action line

The load on the lift line is projected along the z axis and the y axis. The z and y components are

$$f_z(x)=dL(\alpha)\cdot\cos(\alpha+\theta-\frac{\phi_0}{2}) \tag{17}$$

$$f_y(x)=dL(\alpha)\cdot\sin(\alpha+\theta-\frac{\phi_0}{2}) \tag{18}$$

The relationship between x and α is

$$\tan\frac{\phi_0}{2}\cdot(1-\frac{2}{3}\cdot\frac{4x-c_R}{c_R-c_T})=\tan(\frac{\phi_0}{2}-\alpha) \tag{19}$$

Let the force acting on the fixed branch A along z (i.e., the axial direction) be $f_{Az}(x)(p\le x\le p+mc_R)$.

Let the force acting on the fixed branch B along z (i.e., the axial direction) be  .

The following equation can be obtained in static equilibrium:

$$\int_{S_F} f_z(x)dx - \int_{S_B} f_{Bz}(x)dx - \int_{S_B} f_{Az}(x)dx = 0 \quad (20)$$

The moment at any point on the fixed branch A is

$$\sum M_{x_A} = \int_{S_F} f_z(x)xdx - \int_{S_B} f_{Bz}(x)xdx - \int_{S_A} f_{Az}(x)xdx = 0 \quad (21)$$

The load distribution on the fixed branch can be calculated by combining Eqs. (20) and (21).

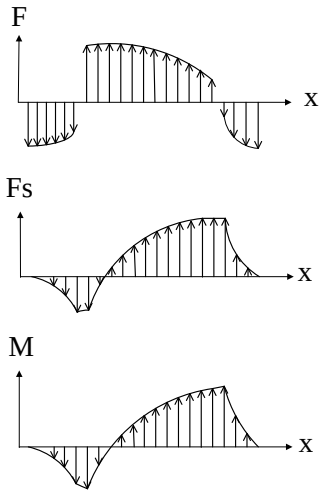

Fig. 3 Load, stress, and torque distributions.

The force can be approximated as a uniform distribution if the width of the fixed branch is much smaller than the width of the root [19]. Eqs. (20) and (21) can be rewritten as follows:

$$\int_{S_F} f_z(x)dx - f_{Az} \cdot S_{Az} - f_{Bz} \cdot S_{Bz} = 0 \quad (22)$$

$$2\int_{S_F} f_z(x)xdx - f_{Az} \cdot mc_R(mc_R + 2p) - f_{Bz} \cdot mc_R(2c_R - 2q - mc_R) = 0 \quad (23)$$

Solving the Eqs. (22) and (23) yields

$$f_{Az} = \frac{\int_{S_F} f_z(x)xdx - (c_R - q - \frac{mc_R}{2})\int_{S_F} f_z(x)dx}{mc_R(mc_R + p + q - c_R)} \quad (24)$$

$$f_{Bz} = \frac{(\frac{mc_R}{2} + p)\int_{S_F} f_z(x)dx - \int_{S_F} f_z(x)xdx}{mc_R(mc_R + p + q - c_R)} \quad (25)$$

Therefore, the bending moment at the failure point in the xz plane is

$$M_{y\max} = \begin{cases} \int_{S_A} f_{Az}(x)xdx \\ \int_{S_B} f_{Bz}(x)(x - c_R + q + mc_R)dx \end{cases} \quad (26)$$

The bending moment at the failure point in the xy plane is

$$M_{z\max} = \begin{cases} \int_{S_A} f_{Ay}(x)xdx \\ \int_{S_B} f_{By}(x)(x - c_R + q + mc_R)dx \end{cases} \quad (27)$$

The synthetic bending moment is

$$M = \sqrt{M_{y\max}^2 + M_{z\max}^2} \quad (28)$$

This yields the stress value at the failure point:

$$\sigma = \frac{6M}{d(mc_R)^2} \quad (29)$$

B. Calculation of torsional stress

The distributed load $dL(\alpha)$ generates a moment at the root of the curved plate, resulting in the following torque distribution:

$$T_x(x) = dL(\alpha) \cdot r\sin\alpha \quad (30)$$

The total torque is found by integrating along the projection of the lift line at the root:

$$T = \int_{S_F} T_x(x)dx \quad (31)$$

The inner bending moment along the exhibition direction can be approximated as being uniformly distributed along the fixed branch portion. According to the equilibrium conditions, we obtain

$$T_{AB} \cdot 2mc = T \quad (32)$$

Therefore, the shear stress on the section of the fixed branch portion should be

$$\tau = \frac{6T_{AB}}{d^2} = \frac{6T}{2mcd^2} \quad (32)$$

C. Example analysis

For the combined bending and torsion moment, the structural failure point is in the two-direction stress state, and the principal stresses should be

$$\left.\begin{matrix}\sigma_1 \\ \sigma_3\end{matrix}\right\} = \frac{\sigma}{2} \pm \frac{1}{2}\sqrt{\sigma^2 + 4\tau^2} \quad (33)$$

$$\sigma_2 = 0 \quad (34)$$

According to third strength theory, the strength condition is

$$\sigma_1 - \sigma_3 = \sqrt{\sigma^2 + 4\tau^2} \le [\sigma] \quad (35)$$

A certain curved plate structure is taken as an example for analysis. Let nc be the distance between the fixed branch portion and the front and rear edges. The structural parameters are shown in Table 1.

TABLE 1
CURVED PLATE STRUCTURE PARAMETERS

Radian ϕ_0	1.57 rad	Thickness d	0.006 m
Curve r	0.061 m	Density	7.9×10^3 kg/m^3

Chord length c	0.155 m

After substituting these parameters into the above equation, we obtain

$$\sigma = 26.22 \cdot \frac{2m+4n-1}{m(m+2n-1)} \cdot V^2 \cdot \delta \tag{36}$$

$$\tau = 573.01 \cdot \frac{1}{m} \cdot V^2 \cdot \delta \tag{37}$$

The following conclusions can be drawn after comparing Eqs. (36) and (37):

1. The torsional stress is the primary factor in strength verification as it is much larger than the bending stress.

2. The structural strength primarily depends on the width of the fixed branch portion, while its position has little effect.

3. The failure stress is proportional to the product of the square of the velocity and the incoming flow angle.

Figure 4 shows the variation in the failure stress as the width of the fixed branch portion, square of the incoming flow velocity, and incoming flow angle change.

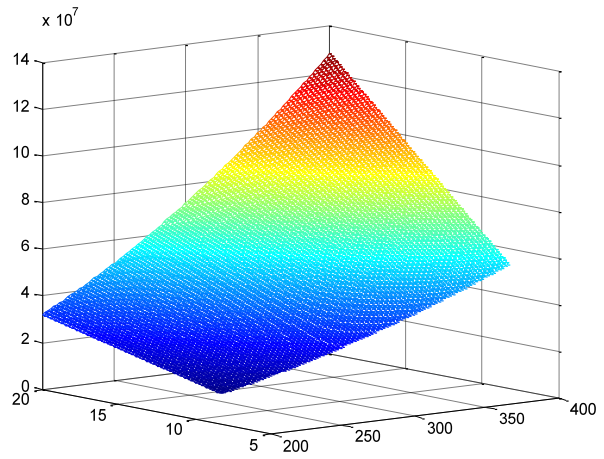

Fig. 4 Variation of the dangerous stress

In order to verify the reliability of the model, the finite element simulation software ANSYS was used to simulate the stress on the cylindrical curved plate under a flow field of 2.5 M_a angled at 4°, as shown in Fig. 5.

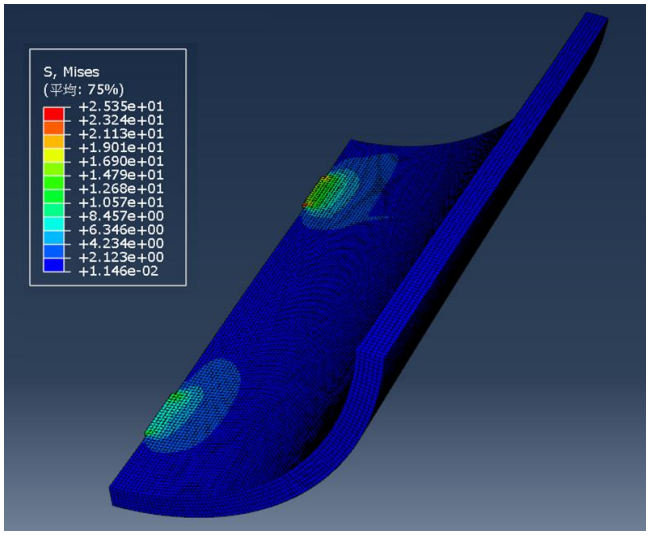

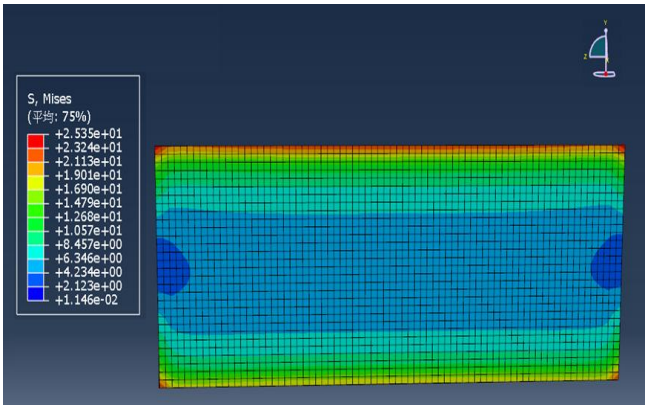

Fig. 5 Simulation of static loading strength

The simulation results show that the failure stress point appears at the vertex of the joint. The stress value is about 25.35 MPa, and the calculated value in the model is 29 MPa; the error is about 14%. This is primarily caused by the theoretical calculation error for the lift line. In practical applications, a certain scale reduction factor can be introduced into the model depending on the actual situation, thus that the calculation result could be more accurate.

V. Dynamic Strength Verification

A. *Empirical formula for dynamic stress*

High speed rotation of the curved plate structure will produce a dynamic load that is much larger than the static load. Therefore, the influence of the dynamic response of the curved plate must be considered during strength verification.

A large number of finite element simulation calculations and experimental results show that the dynamic stress at the failure point has the following relationship with static stress:

$$\sigma_d = K_d \cdot \sigma_j \tag{38}$$

where K_d is the dynamic coefficient, which has a nonlinear relationship with the ratio of the first-order natural frequency f to the rotational speed $\dot{\phi}$ of the curved plate, as shown in Fig. 6:

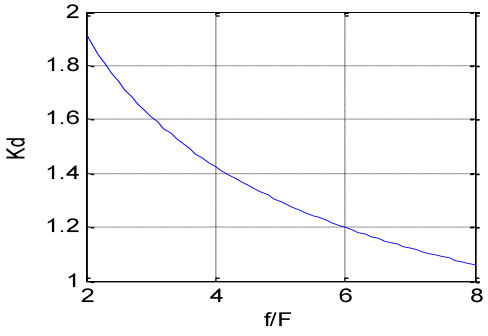

Fig. 6 Dynamic coefficient

The first-order natural frequency of the curved plate can be obtained by correcting the natural frequency equation of the flat plate with one side fixed and three sides free:

$$f = \frac{\Delta}{2\pi} \cdot \frac{a^2}{(\phi_0 r)^2} \cdot \bar{d} \sqrt{\frac{gE}{12(1-\gamma^2)\rho}} \tag{39}$$

where a^2 is a constant. Regarding the first-order natural frequency, a^2 is only slight different when the aspect ratio of the rectangular plates changes, thus we take $a^2 = 3.494$. $\overline{d}$ is the average thickness, g is the gravitational acceleration, E is the modulus of elasticity, γ is Poisson's ratio, ρ is the density, and Δ is the correction factor.

B. Analysis of examples

The previous curved plate model is analyzed here. Figure 7 shows the finite element simulation results of the first three vibration modes of the curved plate. The first order natural frequency was substituted into the model for analysis.

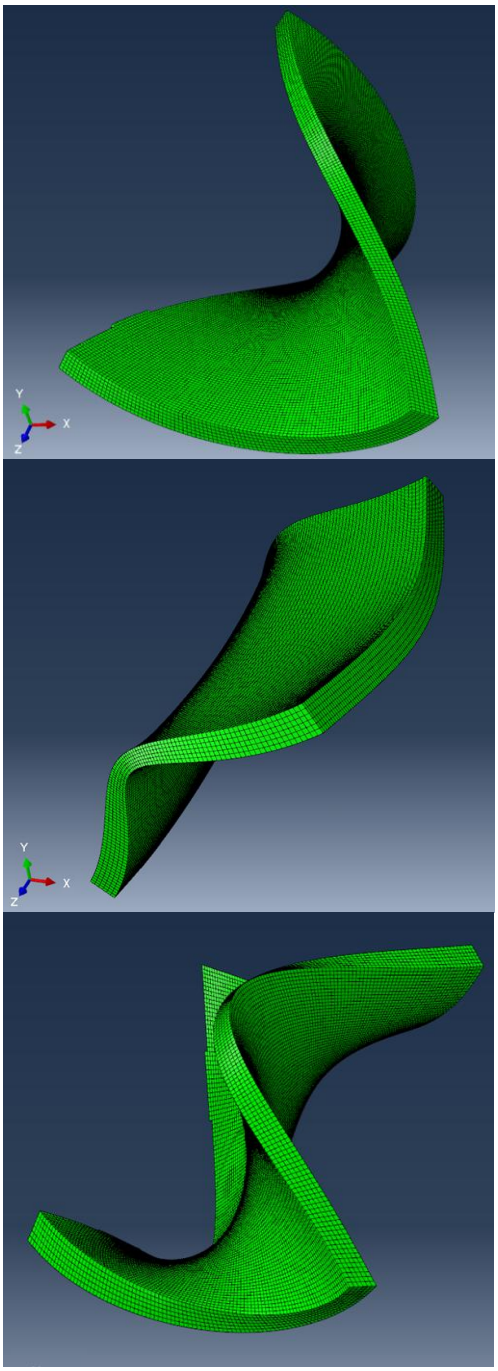

Fig. 7 Finite element simulation of the first three vibration modes of curved plates.

Figure 8 shows the static stress and dynamic stress responses at the failure point for initial speeds of 1100 r/s, 1300 r/s, 1500 r/s, and 1700 r/s.

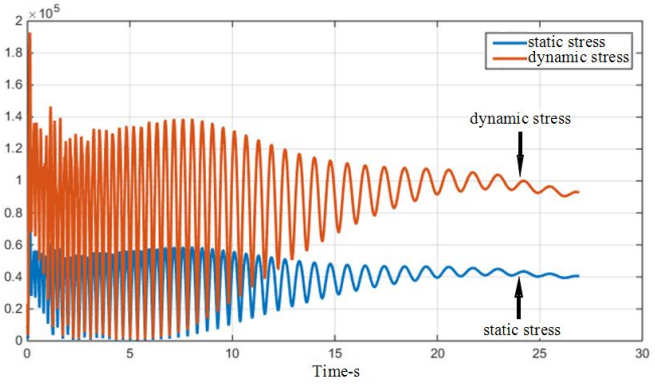

Initial speed: 1100 r/s

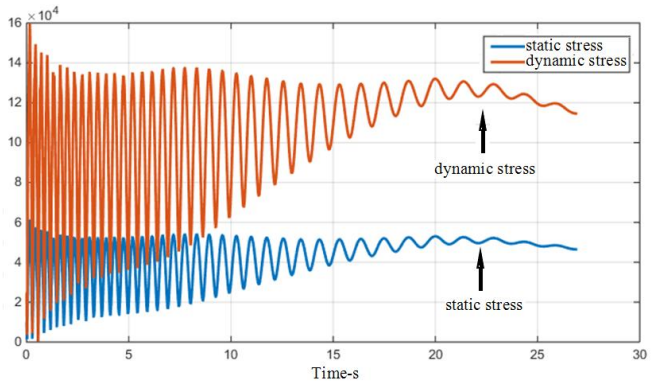

Initial speed: 1300 r/s

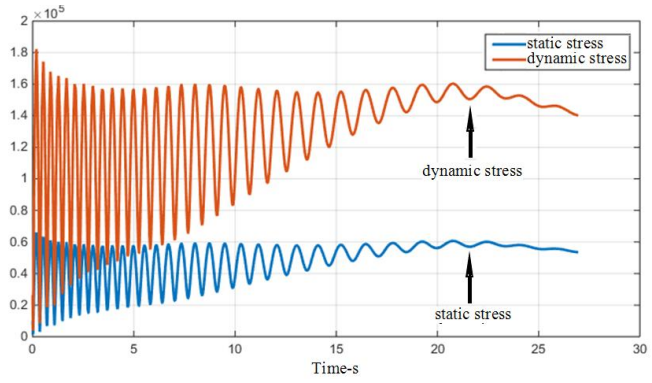

Initial speed: 1500 r/s

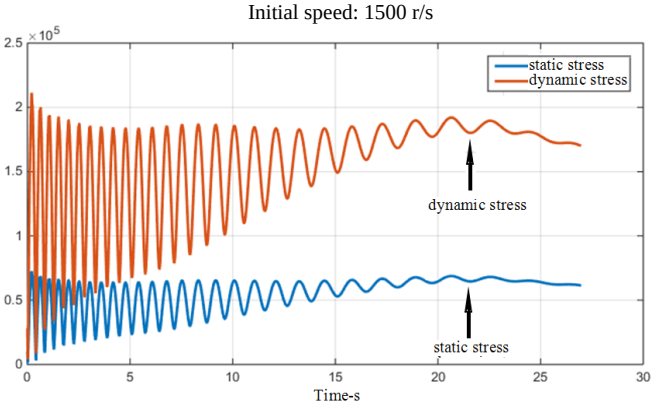

Initial speed 1700 r/s

Fig. 8 Comparison of static stress and dynamic stress responses at different speeds.

The analysis shows that the dynamic stress increases as the rotational speed increases. Based on this variation in the dynamic coefficient variation, it is not surprising that the growth will take the form of an index. Therefore, in order to ensure the structural strength requirements of the curved plate, the rotational speed must be controlled within a certain range in actual applications.

VI. Conclusion

Based on the existing empirical strength verification methods for curved plates, the static and dynamic strength verification methods combined with aeroelastic analysis theory were studied for rotating curved plate structures in a flow field.

First, a unilateral fixed support model of the curved plate was established by simplifying the shape deformation model of the cylindrical curved plate. Based on this, the load redistribution on the curved plate for different flow velocities and directions was solved. A static strength verification model was established based on material mechanics analysis. This method is far more convenient and simpler than the use of numerical methods. According to the analysis and verification of the example, the accuracy can basically meet the requirements of practical applications.

Second, a dynamic stress verification method is presented based on the empirical relationship between the static stress and dynamic stress, and the dynamic stress response of a specific curved plate model under different initial rotational speeds was simulated numerically. The analysis shows that the dynamic stress value of the curved plate will increase exponentially as the rotational speed increases, which provides a theoretical basis for strength design and analysis of this type of structure.

In the stereotyped test of a certain type of rocket, there have been many ballistic mid-fall accidents. By comparing with the debris recovered from previous tests, it was found that the wings were unusually damaged. Through the analysis of the data recorded by the missile sensor, it was found that during the rocket flight, the abnormal speed accelerated dramatically, and the load on the wings increased sharply accordingly, and the structure was destroyed, eventually leading to flight instability. After the overall redesign of the rocket, the speed during its flight is kept within a certain range, and such problems have been solved.

References

[1] Zhou J. Yang Z C. He S. Static pressure modification for piston theory aerodynamics and its application to the analysis of curved panel flutter. Acta Aeronautica et Astronautica Sinica, 2013, 34(7): 1512-1519

[2] FANG Li-qing; ZHANG Lei Modeling and experiments of equivalent viscous damping for piezoelectric unimorph cantilevers [J] Optics and Precision Engineering 2014.22(3)641-647

[3] Narimani E, Shahhoseini S. Optimization of vane mist eliminators [J]. Applied Thermal Engineering, 2011, 31: 188-193

[4] WANG Long-kai, BIN Guang-fu, LI Xue-jun, LIU Ding-qu. Effects of unbalance Location on dynamic characteristics of high-speed gasoline engine turbocharger with Floating Ring Bearings [J]. Chinese Journal of Mechanical Engineering. 2016 (02)

[5] ZHU L, YU Y, WANG H. Effect of defects in cylindrical panels and fix-errors on buckling behavior [J]. Acta Aeronauticaet Astronautica Sinica, 2016,37(7):2180-2188

[6] Redshaw S C. The elastic instability of a thin curved panel subjected to an axial thrust, its axial and circumferential edges being simply supported[R]. Greenwich: British Aeronautical Research Council, 1934

[7] Timoshenko S P, Gere J M. Theory of elastic stability [M]. New York: Mc Graw-Hill,1961:462-468

[8] LE TRAN K, DAVAINE L, DOUTHE C. et. Stability of curved panels under uniform axial compression [J]. Journal of Constructional Steel Research, 2012, 69(1):30-38

[9] Martins J P, Da Silva L S, Reis A. Eigenvalue analysis of cylindrically curved panels under compressive stresses-Extension of rules from EN 1993-1-5[J]. Thin-Walled Structure, 2013, 68:183-194

[10] Shariati M. A numerical and experimental study on bucking of cylindrical panels subjected to compressive axial load [J]. Strojniki Vesthik-Journal of Mechanical Engineering, 2010,56 (10):609-618

[11] HAN Zi-jian, XUE Yinian, HAN Jinhu, et al. Internal pressure test of cylindrical panels [J]. Mechanics in Engineering, 1980(1):46-48.

[12] Sun L Y, Yu Y, Chen B, et al. A new method for implementation of simple supported boundary in stability test of cylindrical panel under axial compression[J]. Journal of Mechanical Engineering, 2014, 50(8): 53-58

[13] Li C, Wu Z. Buckling of 120° stiffened composite cylindrical shell under axial compression- experiment and simulation [J]. Composite Structure, 2015, 128: 199-206

[14] CHEN Huanxing, XUE Kexing. Buckling test of integral stiffened waffle cylindrical panels[J]. Acta Mechanica Solida Sinica, 1982(2):236-246.

[15] Vescovini R, BIsagni C. Buckling analysis and optimization of stiffened composite flat and curved panels [J]. AIAA Journal, 2012,50(4):904-915

[16] FAN Qinshan, CHEN Wen. Initial postbuckling and imperfection sensitivity of a cylindrical shell [J]. Journal of Tsinghua University, 1990, 30(2):76-83.

[17] WU Hongfei, YUAN Shijian, WANG Zhongren, et al.Effect of initial defects and proportional loading paths on the elastoplastic stability of cylindrical shell[J]. Chinese Journal of Mechanical Engineering, 2003, 39(2):53-57.

[18] Martins J P, Beg D, Sinur F, et al. Imperfection sensitivity of cylindrically curved steel panels [J]. Thin-Walled Structures, 2015,89: 101-115

[19] Huang-Yi Analysis on the wind-induced vibration response and overall stability of large-span timberwork single-layer spherical reticulated shell [D]. Chongqing University 2014

[20] Wang Cun-Fu, Zhao-Min, Ge-Tong. Study on the topology optimal design of under water presser structure [J]. Engineering Mechanical, 2015(1): 247-256

[21] Huang Jin-Qiang, Chen-Jie. Strength and buckling analysis of ring-stiffened cylindrical shell with flat ribs [J]. Ship Science and Technology 2015(9): 7-11

[22] Li Xiao-guang, Li Ming-xing. Engineering Calculation Method of WAF Strength [J] Journal of Ordnance, 1995 9(1):37-39

[23] J.R.Wright, J.E. Cooper. Introduction to Aircraft Aeroelasticity and Loads [M]. Shanghai Jiaotong University Press. 2010